Analysis on Co-channel Interference of Human Body Communication Supporting IEEE 802.15.6 BAN Standard

Jung-Hwan Hwang, Tae-Wook Kang, Youn-Tae Kim, and Seong-Ook Park

Human body communication (HBC) is being recognized as a new communication technology for mobile and wearable devices in a body area network (BAN). This paper presents co-channel interference experienced by HBC supporting the physical layer in the IEEE 802.15.6 BAN standard. To analyze the co-channel interference, a co-channel interference model is introduced, and space-domain and time-domain parameters representing an interference environment are generated using the co-channel interference model. A new signal-to-interference ratio (SIR) parameter depending on the peak amplitudes of the data signals causing co-channel interference is defined; co-channel interference can be easily analyzed and modelled using the newly defined SIR. The BER degradation model derived using the co-channel interference model and SIR in this paper can be effectively used to estimate the performance.

Keywords: Human body communication, co-channel interference, BER degradation.

Manuscript received Aug. 27, 2014; revised Jan. 5, 2015; accepted Jan. 17, 2015.

This work was supported by the Ministry of Knowledge Economy (MKE), Rep. of Korea (100-385-99).

Jung-Hwan Hwang (jhhwang@etri.re.kr) is with the Broadcasting & Telecommunications Media Research Laboratory, ETRI, and the Department of Electrical Engineering, KAIST, Daejeon, Rep. of Korea.

Tae-Wook Kang (twkang@etri.re.kr) is with the SW & Contents Research Laboratory, ETRI, Daejeon, Rep. of Korea.

Youn-Tae Kim (petruskim@chosun.ac.kr) is with the Department of IT Fusion Technology, Chosun University, Gwangju, Rep. of Korea.

Seong-Ook Park (corresponding author, soparky@kaist.ac.kr) is with the Department of Electrical Engineering, KAIST, Daejeon, Rep. of Korea.

I. Introduction

Human body communication (HBC) uses the human body, whose tissues have the features of a lossy dielectric material, as a transmission channel to transmit data between devices, allowing those devices to communicate without wire or wireless connections [1]. As mobile devices, such as smart phones, smart watches, and smart glasses, are gradually becoming necessities in our lives, various context-aware services using such mobile devices are being introduced. HBC is being recognized as an intuitive connection method that enables mobile devices to communicate with each other or with peripheral devices; more versatile services can be provided from such intuitive connections. Along with enabling intuitive communication, HBC technology consumes less power while supporting high data rates of more than 1 Mbps [2]–[7] because a baseband signal is transmitted through the body channel (that is, the human body) without modulation to transform a baseband signal into a pass-band one at an IF or RF band. On account of the low power consumption of HBC technologies, HBC has been applied to data communication for capsule-type endoscopes [8]. Along with hardware development for HBC, the IEEE 802.15 working group for BAN recently published a standard for physical layers (PHYs) using HBC [9]. In HBC PHY, a 4-bit data (that is, a symbol) is converted into a Walsh code composed of 16 chips. The converted code is then spread in the frequency domain using a frequency-selective (FS) spreader and frequency-selective code (FSC), and the resulting baseband signal is transmitted through the human body after mask filtering is conducted to satisfy the

spectral mask.

The tissues composing the human body have a high dielectric constant in a low-frequency band under 100 MHz [10]; hence, the human body functions as an antenna [11]–[12]. The antenna function of the human body causes interference when more than one HBC user exists in proximity; that is, co-channel interference. Part of the baseband signal transmitted through the human body is radiated from the HBC user in a type of electromagnetic wave. The radiated electromagnetic wave is received by another HBC user through the human body; thus, it generates an interference signal at the body channel of this HBC user [13]. An interference signal caused by an HBC user has the same frequency band as the data signal (that is, the baseband signal) transmitted through the body channel experiencing interference because HBC PHY supports only a single-frequency channel at 21 MHz [9]; hence, the interference signal causes co-channel interference. Co-channel interference affects BER performance more strongly than thermal noise, which will be explained later. Co-channel interference can be well investigated to evaluate BER performance in a more realistic way and accordingly, achieve a reliable communication. However, co-channel interference in HBC has not yet been investigated. A baseband signal supporting HBC PHY of the IEEE 802.15.6 BAN standard has a partial periodic characteristic, in which the signal periodicity is maintained in separated time intervals, not in one whole time interval. A data signal causing co-channel interference has sampled-amplitudes (that is, amplitudes where the data signal has at-sampling points) at a receiver. The sampled-amplitudes over a time interval where the partial periodicity is maintained are dependent on each other due to the partial periodicity. If multiple interferers exist, and accordingly, many data signals cause co-channel interference at the same time, then constructive interference between the sampled-amplitudes of each data signal can occur at consecutive sampling points, in which the occurrence of constructive interference is dependent on the time-delay (that is, phase) conditions of the interferers. Interferers causing co-channel interference are distributed, having a random distance from a receiver to be interfered with, and thus each data signal causing co-channel interference has a different amplitude at the receiver; data signals causing co-channel interference have a non-equal amplitude at the receiver to be interfered with. The BER degradation experiences a drastic change when the effect of the interferer's distribution is combined with constructive interference. Co-channel interference, simultaneously depending on the time delay and the distribution of the interferers, makes it more difficult to model the interference phenomenon, because such interference becomes a multi-dimensional phenomenon in which a space-domain parameter (that is, the distribution of interferers) and a time-domain parameter (that is, time delays of interferers) are simultaneously involved.

This paper presents a BER-degradation analysis for co-channel interference that occurs when multiple HBC users exist at the same time. To model complicated multi-dimensional interference, a co-channel interference model is introduced. Using the simulated BER performance, the effects of the space-domain and time-domain parameters on BER degradation are analyzed. To simplify the BER-degradation analysis, an SIR parameter is newly defined, which is dependent on the peak amplitudes of the data signal causing co-channel interference, and accordingly, easily obtainable using the distribution of HBC users. The BER degradation model having such SIR as an independent variable is derived with respect to an HBC application. The derived BER degradation can be effectively used to estimate BER degradation in a real interference environment.

II. Co-channel Interference Model

The antenna function of the human body causes co-channel interference, especially when multiple HBC users exist in proximity to each other, as shown in Fig. 1. Data signals radiated from HBC transmitters owing to the radiating characteristic of the human body are propagated through free space to an HBC user experiencing interference. The propagated data signals are then received by the HBC user owing to the receiving characteristic of the human body. Interference accordingly occurs at the HBC receiver of the HBC user because the HBC receiver receives data signals for other HBC users along with the desired signal that is

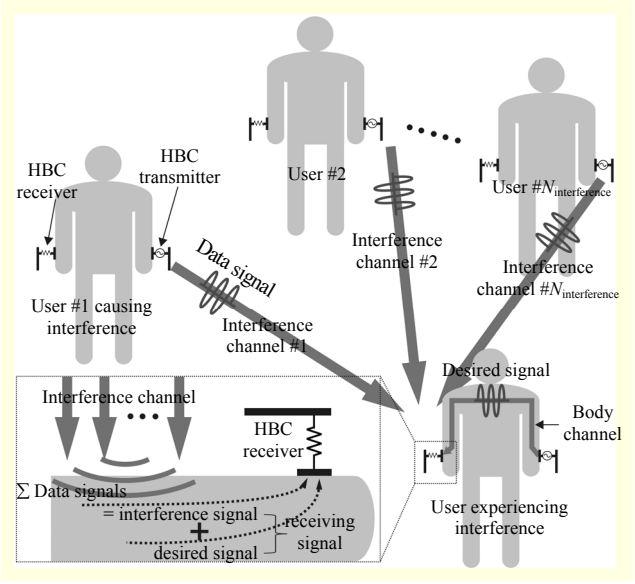

Fig. 1. Co-channel interference in HBC.

ETRI Journal, Volume 37, Number 3, June 2015
http://dx.doi.org/10.4218/etrij.15.0114.1029

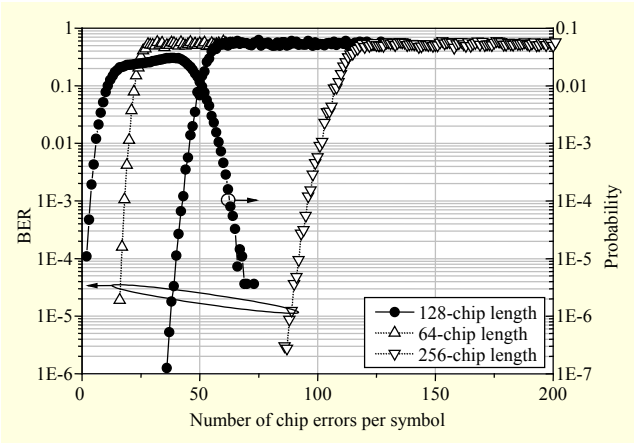

Fig. 2. BER according to number of chip errors and distribution of number of chip errors.

transmitted from the HBC transmitter of the same HBC user. When multiple HBC users exist, the data signals for other HBC users are added at the HBC receiver, and finally, the added data signals become an interference signal. An interference signal generated in such a way causes co-channel interference because the interference signal occupies the same frequency band as the desired signal. In this paper, the body channel is defined as a transmission channel that is formed inside the human body of an HBC user. Desired signals are transmitted through the body channel. Different from the body channel, the interference channel is defined as a transmission channel that is formed outside the human body (that is, between HBC users). A data signal is sequentially radiated from one HBC user and then propagated and received by another HBC user through the interference channel between two HBC users, as shown in Fig. 1; accordingly, an interference signal is received along with a desired signal. HBC PHY in [9] transmits the spread Walsh codes; hence, a receiving signal can be correctly decoded when an error caused by an interference signal occurs at several chips in one Walsh code. Decoding, however, is impossible when an error occurs at too many chips. Figure 2 shows the simulation results for the change of the BER performance according to the number of error chips occurring in one symbol. In the simulation, chip errors corresponding to the abscissa were generated in each symbol. For this, a randomly generated 4-bit symbol was converted into a 128-chip Walsh code according to the frequency selective digital transmission (FSDT) scheme [9]. After a total of 10^6 symbols were converted, an error was generated with respect to randomly selected chips within each symbol, and each Walsh code corrupted by errors was then decoded into a 4-bit symbol. When an error occurs at less than 36 chips, a symbol error does not exist in the decoded symbol; however, a symbol error starts to occur, and accordingly, a BER performance is degraded when an error occurs at more chips. The same phenomenon is observed with respect to a Walsh code of different chip length. As shown in Fig. 2, a symbol error occurs when an error occurs at over 16 and 86 chips with respect to the 64- and 256-chip-length Walsh code, respectively. Due to the minimum distance of the Walsh code, the BER curve shifts while maintaining a similar pattern, as the length of the Walsh code increases.

Figure 3(a) shows the simulated signal pattern for a data signal before and after mask filtering to satisfy the spectral mask defined in [9]. Harmonic components of the data signal were removed by mask filtering; thus, the data signal in the time domain did not have high-frequency components after the mask filtering. The FSC is composed of periodic chips toggling alternately between "0" and "1" for its length [9]. The data signal before mask filtering is composed of FSCs continuing one after another, as shown in Fig. 3(a). During mask filtering, the number of occurrences of the complete removal of signal components from the periodic chips is reduced, because these signal components are mainly distributed near the center frequency of 21 MHz; hence, the data signal after mask filtering still maintains its periodicity and amplitude in the time intervals corresponding to the central part of the FSC, as shown in Fig. 3(a). A constant periodicity and amplitude were maintained in a long time interval when the same FSCs continued in the data signal, as shown in the lower part of Fig. 3(a). Contrary to this, the number of occurrences of the complete removal of signal components from the periodic chips is increased by mask filtering because these signal components are distributed at values below 21 MHz (that is, approximately half of 21 MHz); hence, the data signal after mask filtering did not maintain its periodicity and amplitude in the time intervals corresponding to the same chips, as shown in Fig. 3(a). In one FSC, the time interval in which the same chips continue is much shorter than that corresponding to the central part of the FSC; moreover, no time interval in which the same chips continue exists as long as the same FSCs continue. For these reasons, a data signal before mask filtering has time intervals of the same chips continuing less frequently, and accordingly, a data signal nearly always maintains its periodicity and large amplitude even after mask filtering. A data signal causing co-channel interference maintains a large amplitude in many time intervals; BER degradation is mainly determined by error occurrence in these time intervals because the large amplitude of a data signal causing co-channel interference leads to error occurrences with high probability. A large amplitude is accompanied by periodicity; thus, the main signal components are distributed near the center frequency in time intervals that have a large amplitude. Although BER degradation at an HBC receiver is affected by the signal loss of

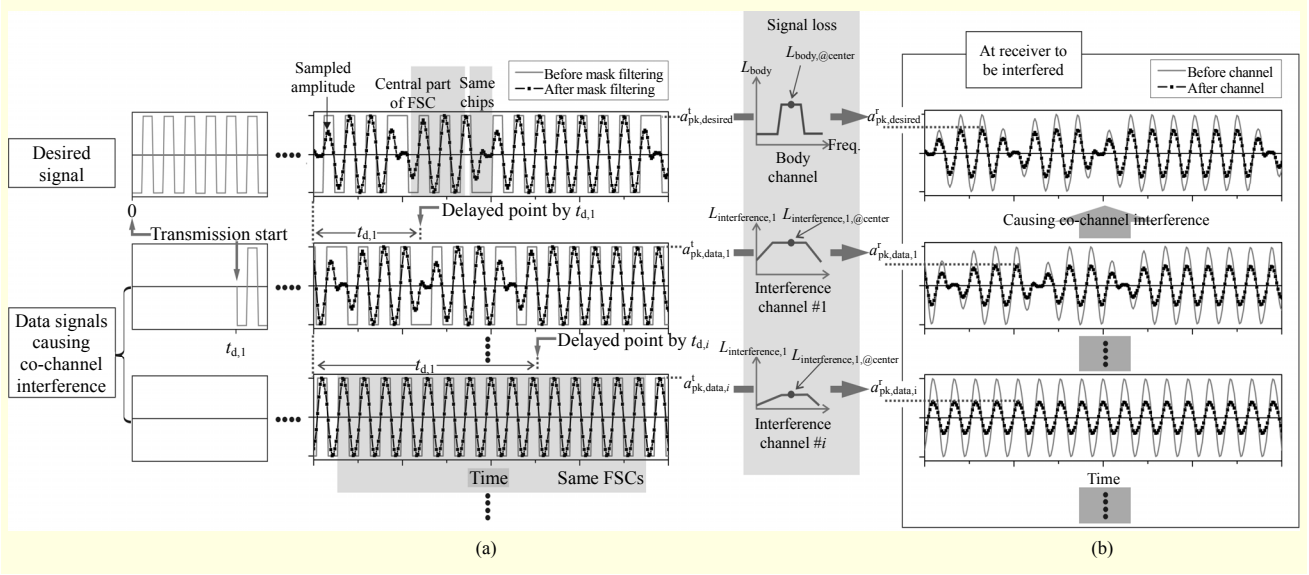

Fig. 3. Signal pattern of data signal at: (a) HBC transmitter and (b) receiver.

the body and interference channels, it is mainly affected by the signal loss at the center frequency because the main signal components are distributed near the center frequency. In HBC, an electrical signal is transmitted through the human body from an HBC transmitter, and a voltage signal that is induced at the signal electrode of the HBC receiver owing to the transmitted electrical signal is then detected [9]. Therefore, it is more convenient to represent the desired and interference signals with amplitude in volts, and channel signal-loss is represented, accordingly, by amplitude loss. As shown in Fig. 3, L_{body} and $L_{interference,i}$ are defined, respectively, as the amplitude loss of the body and the ith interference channel in the linear scale. In addition, L_{body} and $L_{interference,i}$ at the center frequency are, respectively, defined as $L_{body,@center}$ and $L_{interference,i,@center}$. At a HBC transmitter, positive peak amplitudes of a desired signal to be transmitted through the body channel and a data signal to be transmitted through the ith interference channel are, respectively, defined as $a^{t}_{pk,desired}$ and $a^{t}_{pk,data,i}$, as shown in Fig. 3(a). The peak amplitude of each signal before mask filtering is equal to the source amplitude corresponding to the high amplitude of the baseband signal. A transmit filter for mask filtering is designed not to attenuate a signal component at the center frequency of 21 MHz; thus, peak amplitudes before and after mask filtering are almost the same because the peak amplitudes occur in time intervals that maintain the periodicity, as shown in Fig. 3(a). Accordingly, the attenuation level at the center frequency dominantly affects the peak amplitude. At a HBC receiver, positive peak amplitudes of the desired and data signals after transmission through the body and the ith interference channels are, respectively, defined as $a^{r}_{pk,desired}$ and $a^{r}_{pk,data,i}$ as shown in Fig. 3(b). Here, $a^{r}_{pk,desired}$

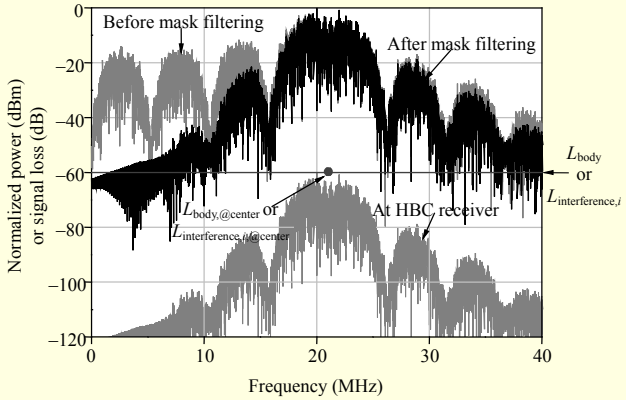

Fig. 4. Spectrum pattern and signal loss in HBC.

occurs in time intervals that maintain the periodicity; hence, $L_{body,@center}$ dominantly affects $a^{r}_{pk,desired}$: $a^{r}_{pk,desired} = a^{r}_{pk,desired} \times L_{body,@center}$. Moreover, $a^{r}_{pk,data,i}$ is also obtained in a similar way; that is, $a^{r}_{pk,data,i} = a^{t}_{pk,data,i} \times L_{interference,i,@center}$. Figure 4 shows the spectrum patterns for a data signal before and after mask filtering to satisfy the spectral mask defined in [9]. A data signal after mask filtering does not have significant signal components outside the occupying band, which has a center frequency of 21 MHz and a bandwidth of 5.25 MHz. BER degradation is not greatly affected even if the signal loss of the body and interference channels outside the occupying band is assumed to have the same value as that over the occupying band, because the signal components that dominantly determine the BER degradation are mainly distributed near the center frequency. The signal loss over the occupying band can be assumed to have a constant value because all of the

simulated signal losses in [13] show an almost constant value over the occupying band. Similar results are observed in [14], in which the simulated signal loss shows little variation, less than 3 dB, over the occupying band, and the variation has the smallest value at a transmission distance of 120 cm. Therefore, the signal loss of the body and interference channels can be assumed to have a constant value over the whole frequency band. In this paper, L_{body} and $L_{interference,i}$ have a constant value equal to $L_{body,@center}$ and $L_{interference,i,@center}$, respectively; hence, the spectrum pattern for a data signal at the HBC receiver is scaled down by $L_{body,@center}$ or $L_{interference,i,@center}$, as shown in Fig. 4, in which a 60 dB signal loss is assumed as an example. In addition, it can be assumed that the interference channel does not cause multipath effects, because the signal components transmitted through the interference channel are distributed at a low frequency of 21 MHz, and accordingly, the wavelength of the signal components is considerably larger than the physical size of surrounding objects, which can cause reflection or diffraction.

The co-channel interference model generates parameters that represent a co-channel interference environment, and at the same time, affect the BER performance at the HBC receiver; simulation of BER degradation is conducted using the generated parameters. The power of an interference signal affecting the BER performance is dependent on two factors: the distance between HBC users causing and experiencing co-channel interference and the arrival time of data signals at an HBC receiver experiencing co-channel interference. Data signals causing co-channel interference are propagated through the respective interference channel, as shown in Fig. 1; thus, the power of an interference signal is dependent on the distance between HBC users causing and experiencing co-channel interference. A received signal, including an interference signal, is sampled at an HBC receiver experiencing co-channel interference; therefore, the power of the interference signal is also dependent on the arrival time of the data signals causing the co-channel interference at the HBC receiver. Data signals causing co-channel interference arrive at the HBC receiver at variable arrival times because the HBC transmitter randomly starts to radiate the data signal, causing co-channel interference, as shown in Fig. 3(a). A data signal causing co-channel interference is sampled along with the desired signal during the process for recovery of the transmitted data; sampled-amplitudes of the data signal change according to the arrival time at the HBC receiver, even if the data signal has the same pattern before the sampling; this is because a data signal has a different amplitude at a specific sampling point according to when the data signal arrives at the specific sampling point. Owing to such variable sampled-amplitudes, a data signal (that is, an interference signal) has a different power according to its arrival time at an HBC receiver. When more than two data signals cause co-channel interference at the same time, the effect of the arrival time on the power of an interference signal becomes more complicated because data signals received at an HBC receiver have a peak amplitude at almost the same time, depending on the arrival time of each data signal, and accordingly, constructive interference between data signals occurs. An interference signal resulting from the addition of data signals under constructive interference has a large amount of power, and accordingly, severely degrades the BER performance, as in the case of a short distance between HBC users. As a result, the power of an interference signal is simultaneously dependent on the distances between the HBC users (that is, the distances of the interference channels) and the arrival time of the data signals. Each data signal causing co-channel interference and the desired signal, respectively, have specific arrival times differing from each other; this is equivalent to the idea that a data signal is delayed by a time delay corresponding to a difference in the arrival time when the desired signal is fixed, as shown in Fig. 3(a). The co-channel interference model generates the distance and time delay of each interference channel.

1. Transmission Distance of Interference Channel

The transmission distance of the ith interference channel, which is equal to the physical distance between HBC users causing and experiencing co-channel interference on the ith interference channel, is defined as $d_{user,i}$. In the co-channel interference model, $d_{user,i}$ is modeled to be uniformly distributed because the HBC users causing co-channel interference exist randomly around the HBC user experiencing co-channel interference.

The amplitude loss of the interference channel is dependent on $d_{user,i}$. The relation between interference channel loss and $d_{user,i}$ can be easily generalized because interference channel loss is caused by wave propagation, and accordingly, its dependency on the distance follows the path loss model for free space. If $L_{interference,i,@center}$ is measured or simulated when HBC users, respectively, causing and experiencing co-channel interference stay away from each other at a reference distance, $d_{user,ref}$, then the loss at another distance can be derived using the amplitude loss at $d_{user,ref}$ and the change in loss caused by the difference from $d_{user,ref}$, in which the amount of change follows the path loss model for free space; hence, $L_{interference,i,@center}$ is expressed as

$$L_{\text{interference},\, i,\, @\,\text{center}} = L_{\text{ref},\, i} + 10n\log\left(\frac{d_{\text{user, ref}}}{d_{\text{user},\, i}}\right). \qquad (1)$$

Here, $L_{ref,i}$ represents $L_{interference,i,@center}$ at $d_{user,ref}$, and

$L_{\text{interference},i,@\text{center}}$ and $L_{\text{ref},i}$ are measured in the unit of dB. The second term in (1) is the log-distance path loss, which represents the amount of change in the amplitude loss according to the transmission distance. In addition, n is the path loss exponent, whose value is dependent on the propagation environment of the interference channel, and $L_{\text{ref},i}$ can be obtained from measurement or simulation after $d_{\text{user,ref}}$ is determined. For this, the amplitude loss of the interference channel is obtained at the center frequency when another HBC user causing co-channel interference exists at a distance of $d_{\text{user,ref}}$; $L_{\text{ref},i}$ is equal to the obtained $L_{\text{interference},i,@\text{center}}$. The amplitude loss of the interference channel is dependent on the direction in which the co-channel interference occurs; it has a different value depending on the incident angle of the wave propagation causing the co-channel interference. The dependency on the incident angle, however, is ignored in this paper because a data signal propagated through an interference channel has low-frequency components, and accordingly, the wave propagation does not have a high directivity. Therefore, $L_{\text{ref},i}$ has the same value, L_{ref}, for all interference channels because the corresponding transmission distances are the same as $d_{\text{user,ref}}$, and accordingly, $L_{\text{ref},i}$ also has the same value, L_{ref}. After L_{ref} is obtained, $L_{\text{interference},i,@\text{center}}$ is calculated from the corresponding $d_{\text{user},i}$.

2. Time Delay of Interference Channel

In the co-channel interference model, the arrival time of a data signal causing co-channel interference is represented using a time delay. On the body and interference channels, each data signal has a specific arrival time that differs from the others owing to a data transmission having a random starting time; this is equivalent to delaying a data signal on the interference channel, as shown in Fig. 3(a), after assuming that it is synchronized with the desired signal before mask filtering is applied. In Fig. 3(a), $t_{\text{d},i}$ represents the time delay of a data signal to be transmitted through the ith interference channel. In this way, a data signal transmitted through the ith interference channel causes co-channel interference when it is not synchronized with the desired signal; in this relation, the degree of non-synchronization is controlled by $t_{\text{d},i}$. Data signals radiated from each HBC user experience a propagation delay during their propagation through the interference channel; however, such a propagation delay can be ignored because its size is relatively smaller than the time delay caused by the random starting time of a data transmission. An HBC transmitter starts to transmit a data signal, and accordingly, the data signal is randomly delayed with respect to the desired signal; hence, the time delay of the interference channel is modeled to be uniformly distributed, such as with $d_{\text{user},i}$.

III. Analysis of Co-channel Interference in HBC

In co-channel interference, BER degradation depends on the space- and time-domain parameters; such dependency is investigated using BER samples obtained through a simulation.

1. Characteristic of BER Distribution

Here, $a^{\text{t}}_{\text{pk,desired}}$ and all $a^{\text{t}}_{\text{pk,data},i}$s were determined to be 1 V during the simulation to obtain the BER samples. In addition, L_{body} and $L_{\text{interference},i}$ were determined using the simulation results in an earlier study [13], in which the main signal and separation distance are equal to the desired signal and $d_{\text{user},i}$, respectively, in this paper. In [13], only the power of the desired and interference signals at the receiver was simulated; however, the signal loss of each signal can be obtained using the power at the transmitter, which was equal to 0 dBm. In this paper, it was assumed that the transmitter and receiver on the body channel are located on each hand, and accordingly, the transmission distance is about 150 cm; hence, $L_{\text{body},@\text{center}}$ was determined using the signal loss simulated under the same condition in [13]; $l_{\text{body},@\text{center}}$ was equal to the simulated signal loss at the center frequency, which is 21 MHz, when the transmission distance is about 150 cm. Moreover, $d_{\text{user,ref}}$ in (1) was set at 10 cm, and $L_{\text{ref},i}$ in the same equation was determined using the simulated signal loss of the interference signal in [13]; $l_{\text{ref},i}$ was equal to the simulated signal loss of the interference signal at the center frequency when $d_{\text{user},i}$ (that is, the separation distance) was 10 cm, because $L_{\text{ref},i}$ is equal to $L_{\text{interference},i,@\text{center}}$ at $d_{\text{user,ref}}$. In the simulation, the symbol rate and spreading factor (that is, the length of FSC) in the FSDT scheme were set at 328 kbps and 8 cm, respectively, to achieve the highest data rate of 1.3125 Mbps, as indicated in [9]. In order for mask filtering to satisfy the spectral mask defined in [9], a generated data signal was sampled with a sampling frequency of 336 MHz; the oversampled data signal was then filtered using a transmit filter. At the HBC receiver, a receiving data signal was downsampled with a downsampling rate of 8; thus, the sampling frequency decreased to 42 MHz. The sampled data signal was then demodulated using the maximum likelihood detection method under the assumption that the timing synchronization between the HBC transmitter and the receiver is perfect [3].

Using the determined variables for the simulation, the BER samples were obtained. To investigate the effect of the time-domain parameter on the BER distribution, a total of 1,000 BER samples were obtained through a simulation in which multiple $t_{\text{d},i}$s of interference channels were randomly generated using the co-channel interference model. A frequency histogram representing the resulting BER distribution was then

obtained using the acquired BER samples. While obtaining the BER samples, $L_{\text{interference},i}$ should be known, because this value determines the interference signal at a receiver. According to (1), $L_{\text{interference},i}$, which was assumed to have a constant value, $L_{\text{interference},i,@\text{center}}$, over the whole frequency band, has a variable value depending on $d_{\text{user},i}$. In the simulation, HBC users causing co-channel interference were located at predetermined locations, and accordingly, each interference channel has a constant $d_{\text{user},i}$; $L_{\text{interference},i,@\text{center}}$ was calculated using $d_{\text{user},i}$s and (1). An interference environment, in which each HBC user is located at $d_{\text{user},i}$, is represented by a distance vector composed of $d_{\text{user},i}$. To investigate the effect of the space-domain parameter (that is, $d_{\text{user},i}$) on the BER distribution, a frequency histogram was obtained under several distance vectors; for this, a total of 1,000 BER samples were repeatedly obtained at each distance vector when randomly generating $t_{\text{d},i}$s. Figure 5 shows the obtained frequency histograms. Each frequency histogram represents a distribution of 1,000 BER samples at a different distance vector; the distance vectors were (100/50/33.3), (100/100/25), and (200/200), for which the numbers in each bracket represent $d_{\text{user},i}$ in cm for each interference channel. Such a distance vector can occur in a real interference environment considering a random distribution of HBC users causing co-channel interference; hence, the frequency histograms obtained do not lose generality. In the simulation, the SNR was –2 dB; therefore, the BER value without an interference signal (hereafter referred to as $\text{BER}_{\text{no-interference}}$) was about 10^{-5}, according to the simulation results for the BER performance determined in an earlier study [15]. Figure 5 also shows the frequency histogram for the same number of BER samples following Gaussian distributions, in which each Gaussian distribution has the same mean and variance as those of the BER samples obtained in the simulation. As can be seen in Fig. 5, the frequency histograms had a wide range with respect to BER; BER had a high value depending on the $t_{\text{d},i}$s. A high BER value, which means a severe degradation in the BER performance, is caused by the constructive interference between data signals. As an example, Fig. 6 shows parts of the interference signals causing BER values of 7.5×10^{-4} and 1.9×10^{-5}, shown in the frequency histogram of Fig. 5(a). The interference signals were obtained after downsampling, while the synchronization condition (that is, $t_{\text{d},i}$s) between the data signals was different. In Figs. 6(a) and 6(b), the sum of the $t_{\text{d},i}$s for all data signals is 6 ns and 29.8 ns, respectively. As the time delays of the interference channels increased from 6 ns to 29.8 ns, the data signals before the mask filtering and the attenuation by the interference channel fell out of synchronization, and accordingly, the BER value decreased sharply to less than about 1/40. When the data signals were close to synchronization, the interference signal had a peak

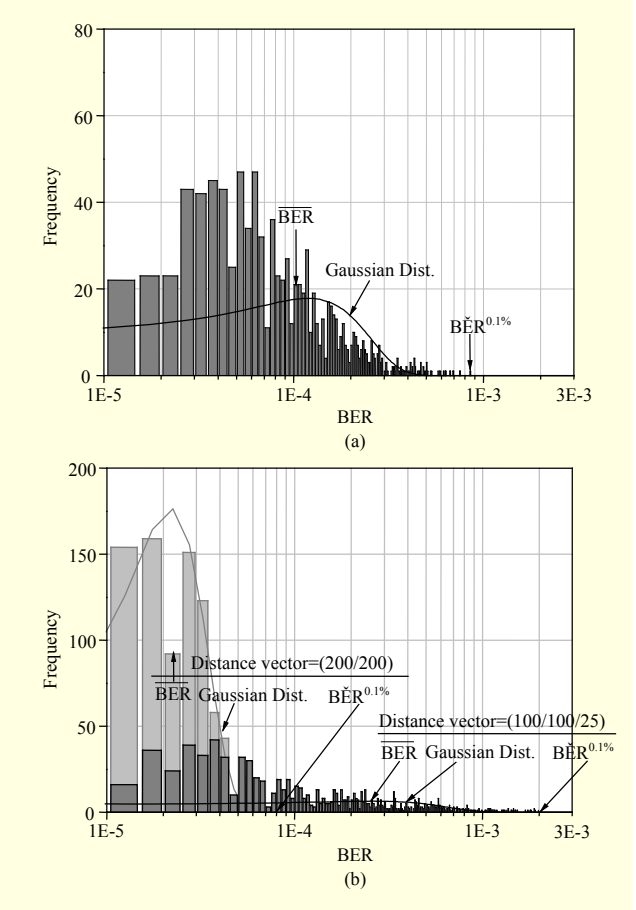

Fig. 5. Frequency histograms of BER samples for $d_{\text{user},i}$s of: (a) (100/50/33.3) and (b) (100/100/25) and (200/200).

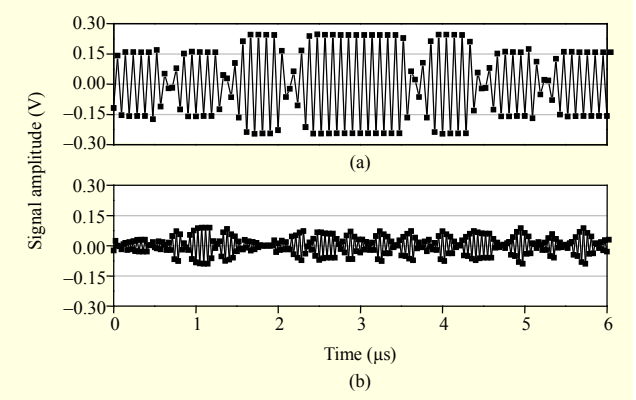

Fig. 6. Interference signal after downsampling causing different BERs of: (a) 7.5×10^{-4} and (b) 1.9×10^{-5}.

amplitude close to the upper limit, which was 0.3 V, and then continuously showed a large peak amplitude, as indicated in Fig. 6(a). The power of the interference signal was high. The interference signal, however, had a small local peak, which did not continue for as long a time interval as in the case of close synchronization, when the data signals were out of

synchronization, as shown in Fig. 6(b); the interference signal shown in Fig. 6(b) has a 10 dB lower power than that shown in Fig. 6(a). Due to the interference signal having such varying power, a receiving data-signal has a varying number of chip errors within one symbol. The number of chip errors occurring within one symbol was simulated using the same simulation variables as those used in Fig. 5(a). Figure 2 shows the distribution of the number of chip errors occurring in one symbol when the 128-chip-length Walsh code is used; the same Walsh code as used in Fig. 5(a), because the FSDT scheme spreads the 16-chip-length Walsh code by using the 8-chip-length FSC [9]. The chip error occurs at about 40 chips in most symbols, whereas it can occur at up to 70 chips when the power of the interference signal is high, as in the interference signal shown in Fig. 6(a). Therefore, the constructive interference causes the severe BER degradation. Along with the frequency histograms, two BER parameters were used to represent a BER distribution: average and worst-case BERs. The average BER, $\overline{\mathrm{BER}}$, was obtained by averaging the obtained BER values. The worst-case BER, $\breve{\mathrm{BER}}^{P_{\mathrm{tail}}}$, was represented by a BER value at an exceedance probability, P_{tail}: $P_{\mathrm{tail}} = \Pr[\mathrm{BER} > \breve{\mathrm{BER}}^{P_{\mathrm{tail}}}] = \int_{\breve{\mathrm{BER}}^{P_{\mathrm{tail}}}}^{\infty} f_{\mathrm{BER}}(x)\,\mathrm{d}x$, where $\Pr[\cdot]$ and $f_{\mathrm{BER}}(x)$ represent the probability and probability density function of a BER distribution, respectively. Here, $\breve{\mathrm{BER}}^{P_{\mathrm{tail}}}$ was estimated using the kth largest BER sample among the obtained BER values, in which P_{tail} is equal to k over the number of obtained BER values. As shown in Fig. 5, $\overline{\mathrm{BER}}$ was almost ten times larger than $\mathrm{BER}_{\text{no-interference}}$ when the distance vector was (100/50/33.3) and (100/100/25), respectively; $\breve{\mathrm{BER}}^{0.1\%}$ (that is, a BER value with P_{tail} of 0.1%) was over eighty times larger than $\mathrm{BER}_{\text{no-interference}}$ while it reached over 10^{-3} when the distance vector was (100/100/25). The BER samples near $\breve{\mathrm{BER}}^{0.1\%}$ had very high BER values, with a much lower frequency than that of the BER samples in other ranges; hence, the BER samples have a non-symmetrical distribution with high skewness. The skewness values of the BER samples shown in Figs. 5(a) and 5(b) when the distance vector is (100/100/25) were 2.2 and 2.3, respectively, which are much higher than that of the Gaussian distribution (that is, 0). Along with the wide range of BER values, the high skewness causes the BER distribution to have a long upper-tail. The long upper-tail of the BER distribution can also be confirmed by comparing the frequency histogram with the Gaussian distribution. A BER distribution is said to have a long upper-tail when it has, at its tail, a probability density higher than the Gaussian distribution. The frequency histogram of the BER samples showed a non-zero frequency at the upper-tail, while the Gaussian distribution had a zero frequency in the same range; hence, the BER distribution has a long upper-tail. As shown in Fig. 5(b), both $\overline{\mathrm{BER}}$ and $\breve{\mathrm{BER}}^{0.1\%}$ had much smaller values as the distance vector changed to (200/200); the length of the upper-tail was at its largest when the distance vector was (100/100/25), while the tail length was at its smallest when the vector was (200/200). As a result, the BER distribution has a dependency on the time-domain parameter, that is, the BER distribution has a long upper-tail, which means a drastic increase in the BER value, depending on the time-domain parameter. It also has a dependency on the space-domain parameter in that the BER distribution has a different tail-length depending on this parameter. When the SNR increases and the corresponding $\mathrm{BER}_{\text{no-interference}}$ becomes smaller than 10^{-5} (for example, 10^{-6}), the power of the thermal noise decreases; the BER distribution has an accordingly longer tail because the co-channel interference affects the BER degradation more strongly. As a result, the long upper-tail characteristic can be generalized for other combinations of relative amplitude losses and higher SNR. A severe BER degradation corresponding to a long upper-tail does not occur frequently, because the BER distribution with a long upper-tail has a relatively low probability density in the range corresponding to the upper tail; however, the BER degradation corresponding to a long upper-tail has a significant effect on the design of the HBC receivers because such receivers experience sudden changes in BER performance once BER degradation occurs.

2. Amplitude-Ratio SIR for Co-channel Interference

When more than one HBC user causes co-channel interference, the space-domain and time-domain parameters become a multi-dimensional parameter, respectively, because multiple $d_{\mathrm{user},i}$ and $t_{\mathrm{d},i}$ values, which are independent of each other, have an effect on the co-channel interference. The BER degradation has a distribution dependent on the multi-dimensional parameters, as shown in Fig. 5. To make it easy to analyze and eventually model such complicated interference phenomenon, the multi-dimensional parameters should be replaced with a scalar quantity. Usually, the SIR is defined as a power ratio of the desired and interference signals at a receiver, which can be used as a scalar quantity to replace the parameters. Owing to the constructive interference, an interference signal has a power level that changes sharply depending on $t_{\mathrm{d},i}$, as shown in Fig. 6. After a BER degradation model having such a power-ratio SIR as an independent variable is obtained through a simulation, in which the SIR has $d_{\mathrm{user},i}$ and $t_{\mathrm{d},i}$ as independent variables, the BER degradation under a real environment of co-channel interference can be estimated using the model after the SIR in a real interference environment is obtained. Such a model, however, is not practical in that $t_{\mathrm{d},i}$ should be exactly

ETRI Journal, Volume 37, Number 3, June 2015
http://dx.doi.org/10.4218/etrij.15.0114.1029

measured to estimate the BER performance, because a change in the SIR according to $t_{d,i}$ is large. The $t_{d,i}$ of each interference channel is easy to change, because it represents the synchronization of the data signal causing co-channel interference with respect to the data signal to be interfered with; such a synchronization condition changes easily depending on the random start time of the data signals. In addition, $t_{d,i}$ has a short duration time (that is, it has various values over a short time period) depending on the HBC application, and if a small amount of data is repeatedly transmitted at a random interval, then $t_{d,i}$ changes instantaneously over a short time period. Therefore, measuring $t_{d,i}$ is not easy. In addition, the measuring of $t_{d,i}$ requires measurement equipment. However, $d_{user,i}$ is a physical parameter that does not change as quickly as $t_{d,i}$ and is easily obtainable without any measuring equipment; hence, a BER degradation model having a $t_{d,i}$-independent SIR as an independent variable is more practical for investigating the BER degradation caused by co-channel interference. In such a BER degradation model, $t_{d,i}$-independent SIR does not represent the BER degradation, which changes depending on $t_{d,i}$; however, a change in BER degradation according to $t_{d,i}$ can be represented by $\overline{\text{BER}}$ and $\breve{\text{BER}}^{P_{\text{tail}}}$, as shown in Fig. 4. After the power of the desired signal is determined (that is, a body channel is fixed), the $t_{d,i}$-independent SIR is dependent only on $d_{user,i}$, in which each value of $d_{user,i}$ determines $L_{interference,i,@center}$ according to (1), and thus $a^{r}_{pk,data,i}$, which is equal to $a^{r}_{pk,data,i} = a^{t}_{pk,data,i} \cdot L_{interference,i,@center}$; hence, $t_{d,i}$-independent SIR becomes the amplitude-ratio SIR. To derive the amplitude-ratio SIR, it is assumed that all data signals are synchronized with each other; and the SIR is then represented by the ratio between the peak amplitudes of the desired and interference signals. Owing to the assumption of synchronization, an interference signal has a peak amplitude equal to the sum of the peak amplitudes that each data signal causing co-channel interference has after being transmitted through each interference channel; hence, the amplitude-ratio SIR can be expressed as

$$\text{SIR} = \frac{a^{t}_{pk,desired} \cdot L_{body,@center}}{\sum_{i=1}^{N_{interference}} a^{t}_{pk,data,i} \cdot L_{intreference,i,@center}}. \quad (2)$$

Here, $N_{interference}$ is the total number of HBC users causing co-channel interference. Using (1), SIR of (2) can be expressed as

$$\text{SIR} = \frac{a^{t}_{pk,desired} \cdot L_{body,@center}}{L_{ref} \sum_{i=1}^{N_{interference}} a^{t}_{pk,data,i} \cdot \left(\frac{d_{user,ref}}{d_{user,i}} \right)^{0.5n}}, \quad (3)$$

where $a^{t}_{pk,desired}$, $a^{t}_{pk,data,i}$, and $L_{body,@center}$ are determined according to the HBC application. After $d_{user,ref}$ is determined, the amplitude loss of the corresponding interference channel, L_{ref}, is measured or simulated. As a result, the SIR of (3) has a variable value depending on the distribution of HBC users causing co-channel interference; the SIR becomes dependent only on $d_{user,i}$s. In the BER degradation model, the SIR is used as an independent variable and BER degradation caused by the asynchronous interference between data signals is represented by $\overline{\text{BER}}$ and $\breve{\text{BER}}^{P_{\text{tail}}}$.

3. BER Degradation Model

Figure 7 shows the simulated BER degradation when the $\text{BER}_{\text{no-interference}}$ value was 10^{-6}. The $\overline{\text{BER}}$ and $\breve{\text{BER}}^{0.1\%}$ values were obtained through a simulation while increasing $N_{interference}$ from two to five. Except for the distance vector and SNR, the simulation conditions were the same as those in Fig. 5. Using the co-channel interference model, a total of 50 distance vectors were randomly generated at each $N_{interference}$, and the BER samples were then obtained at each distance vector while generating $t_{d,i}$s; $\overline{\text{BER}}$ and $\breve{\text{BER}}^{0.1\%}$ were derived using the BER samples at each distance vector, which

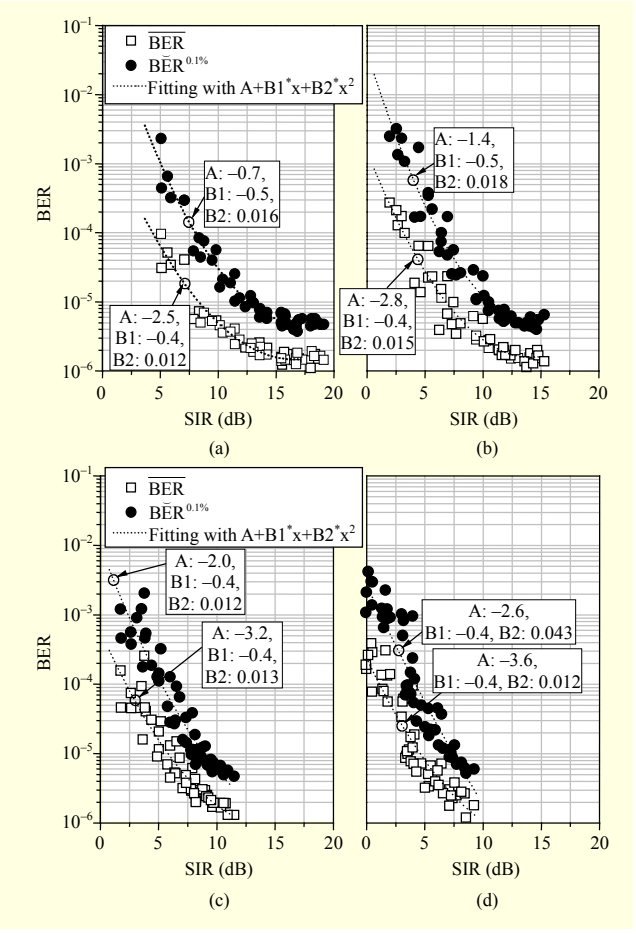

Fig. 7. $\overline{\text{BER}}$ and $\breve{\text{BER}}^{0.1\%}$ when $N_{interference}$ is: (a) 2, (b) 3, (c) 4, and (d) 5.

has a different SIR value according to (3). SNR was determined to be –1 dB, and $BER_{no\text{-}interference}$ was then about 10^{-6} according to the simulation results in [15]; hence, as shown in Fig. 7, $\overline{BER}$ approached gradually to 10^{-6} when the SIR increased over 10 dB, because an interference signal becomes weak and only the thermal noise affects the BER performance. Much higher SIR than SNR is required to achieve a BER of 10^{-6}; it is critical to satisfy an SIR requirement to maintain tolerable BER, because co-channel interference affects the BER performance more strongly than the thermal noise. When the SIR decreased, $\overline{BER}$ and $\breve{BER}^{0.1\%}$ increased gradually, because an interference signal has an increasing power. When the SIR was the same but $N_{interference}$ decreased, $\breve{BER}^{0.1\%}$ generally had an increasing value, because a high BER affecting $\breve{BER}^{0.1\%}$ is caused by constructive interference between data signals; constructive interference occurs with a higher probability when fewer data signals are involved in the co-channel interference. The dependency between SIR and each BER parameter (that is, $\overline{BER}$ and $\breve{BER}^{0.1\%}$) can be modelled by fitting each BER parameter with a second-order polynomial, as shown in Fig. 7, in which the standard deviations of the fitting results were less than 0.3 in all cases. The BER degradation model shown in Fig. 7 can be used to estimate the BER performance in a real interference environment. If the locations of the HBC users causing co-channel interference are determined, then the SIR corresponding to an interference environment can be calculated using (3), because $d_{user,i}$ can be known from the locations of the HBC users; a BER range is then estimated using $\overline{BER}$ and $\breve{BER}^{0.1\%}$ at the calculated SIR (that is, a BER value is distributed around $\overline{BER}$, and in the worst case, around $\breve{BER}^{0.1\%}$) with an exceedance probability of 0.1%. Here, $\breve{BER}^{P_{tail}}$ at a small P_{tail} is useful especially when HBC is used for medical applications [16]–[17] because such applications require highly reliable communication even under co-channel interference, and $\breve{BER}^{P_{tail}}$ at a small P_{tail} is close to an upper bound of the BER performance. Using a BER range estimated using the BER degradation model, the system requirements to maintain reliable data communication even under co-channel interference can be obtained; that is, if a BER range is not satisfied at a particular SIR, then the SIR is increased by increasing $a^{t}_{pk,desired}$ (that is, increasing a transmitting voltage) or decreasing $L_{body,@center}$ (that is, decreasing a transmission distance) until the BER range is satisfied.

IV. Conclusion

This paper presented an analysis of the BER degradation that HBC PHY in IEEE 802.15.6 experiences under co-channel interference. A new SIR parameter was introduced to represent the interference environment with a scalar quantity, which is easily obtainable from a distance vector. In the BER degradation model, the newly-defined SIR, which is dependent on the space-domain parameter, was used as an independent variable; while, the BER degradation dependent on the time-domain parameter at each SIR was represented with $\overline{BER}$ and $\breve{BER}^{P_{tail}}$.

The BER degradation model can be generalized by obtaining the model at various P_{tail} values; in particular, $\breve{BER}^{P_{tail}}$ at a small P_{tail} value is desirable because $\breve{BER}^{P_{tail}}$ approaches an upper bound of the BER performance as P_{tail} decreases. In a real interference environment, the range of SIR can be obtained by investigating the distribution of HBC users causing co-channel interference. Thus, $\overline{BER}$ and $\breve{BER}^{P_{tail}}$ in the obtained SIR range can then be estimated using the BER degradation model after the desired P_{tail} dependent on the HBC application is determined. If the BER performance represented by the estimated $\overline{BER}$ and $\breve{BER}^{P_{tail}}$ is not satisfied, then it can be improved by increasing the SIR, which is determined based on the transmitting voltage and transmission distance.

References

[1] T.G. Zimmerman, "Personal Area Networks: Near-Field Intra-body Communication," *IBM Syst. J.*, vol. 35, no. 3–4, 1996, pp. 609–617.

[2] N. Cho et al., "A 60 kb/s-10 Mb/s Adaptive Frequency Hopping Transceiver for Interference-Resilient Body Channel Communication," *IEEE J. Solid-State Circuits*, vol. 44, no. 3, Mar. 2009, pp. 708–717.

[3] H.-I. Park et al., "Human Body Communication System with FSBT," *IEEE Int. Symp. Consum. Electron.*, Brauschweig, Germany, June 7–10, 2010, pp. 1–5.

[4] T.-W. Chen et al., "A 0.67 mW 14.55 Mbps OFDM-Based Sensor Node Transmitter for Body Channel Communications," *IEEE Asian Solid-State Circuits Conf.*, Jeju, Rep. of Korea, Nov. 14–16, 2011, pp. 189–192.

[5] C.-H. Hyoung et al., "Transceiver for Human Body Communication Using Frequency Selective Digital Transmission," *ETRI J.*, vol. 34, no. 2, Apr. 2012, pp. 216–225.

[6] P.-Y. Tsai et al., "A QPSK/16-QAM OFDM-Based 29.1 Mbps LINC Transmitter for Body Channel Communication," *IEEE Asian Solid-State Circuits Conf.*, Kobe, Japan, Nov. 12–14, 2012, pp. 345–348.

[7] C.K. Ho et al., "High Bandwidth Efficiency and Low Power Consumption Walsh Code Implementation Methods for Body Channel Communications," *IEEE Trans. Microw. Theory Techn.*, vol. 62, no. 9, Sept. 2014, pp. 1867–1878.

[8] IntroMedic, *MicroCam Features*, 2015. Accessed Jan. 28, 2015. http://intromedic.com/eng/sub_products_2.html
[9] IEEE Std. 802.15.6, *IEEE Standard for Local and Metropolitan Area Networks – Part 15.6: Wireless Body Area Networks*, *IEEE*, Piscataway, NJ, USA, 2012.
[10] IFAC-CNR, *Dielectric Properties of Body Tissues*, 1997. Accessed Jan. 28, 2015. http://niremf.ifac.cnr.it/tissprop
[11] J.-H. Hwang et al., "Receptive Properties of the Human Body of Emitted Electromagnetic Waves for Energy Harvesting," *IEEE Antennas Propag. Soc. Int. Symp.*, Chicago, IL, USA, July 8–14, 2012, pp. 1–2.
[12] J.-H. Hwang et al., "Energy Harvesting from Ambient Electromagnetic Wave Using Human Body as Antenna," *Electron. Lett.*, vol. 49, no. 2, Jan. 2013, pp. 149–151.
[13] J.-H. Hwang et al., "Analysis of Signal Interference in Human Body Communication Using Human Body as Transmission Medium," *IEEE Antennas Propag. Soc. Int. Symp.*, Albuquerque, NM, USA, July 9–14, 2006, pp. 495–498.
[14] N. Cho et al., "The Human Body Characteristics as a Signal Transmission Medium for Intra-body Communication," *IEEE Trans. Microw. Theory Tech.*, vol. 55, no. 5, May 2007, pp. 1080–1086.
[15] T.W. Kang et al., "A Complexity-Efficiency Human Body Communications," *IEEE Asia-Pacific Conf. Commun.*, Denpasaar, Indonesia, Aug. 29–31, 2013, pp. 445–446.
[16] D.P. Lindsey et al., "A New Technique for Transmission of Signals from Implantable Transducers," *IEEE Trans. Biomed. Eng.*, vol. 45, no. 5, May 1998, pp. 614–619.
[17] M. Sun et al., "Data Communication between Brain Implants and Computer," *IEEE Trans. Neural Syst. Rehabil. Eng.*, vol. 11, no. 2, June 2003, pp. 189–192.

Jung-Hwan Hwang received his BS and MS degrees in electronic engineering from Chungnam National University, Daejeon, Rep. of Korea, in 1998 and 2000, respectively. From March 2000 to July 2002, he was a research engineer with Knowledge-on Inc., Iksan, Rep. of Korea, working on the development of microwave circuits. Since August 2002, he has been with the Electronics and Telecommunications Research Institute, Daejeon, Rep. of Korea, where he is currently a senior engineer. He has been primarily involved in radio-channel modeling. His research interests include electromagnetic compatibility and health and safety effects of electromagnetic fields.

Tae-Wook Kang received his BS and MS degrees in electrical engineering from Pohang University of Science and Technology, Rep. of Korea, in 2005 and 2007, respectively. Since 2007, he has been with the Electronics and Telecommunications Research Institute, Daejeon, Rep. of Korea, where he is currently a senior engineer with the System Semiconductor Department. He has been primarily involved in wireless communications, human body communications, and power management for energy harvesting systems.

Youn-Tae Kim received his BS and PhD degrees in electronics engineering from Ajou University, Suwon, Rep. of Korea, in 1980 and 1990, respectively. He had been a director with the Human Information and Communication Department, Electronics and Telecommunications Research Institute, Daejeon, Rep. of Korea, where he was working on bio-information and communications; MEMS/NEMS devices; and micro-devices for bio-communications. He is currently a professor with both the Department of Electronic Engineering and the Department of IT Fusion Technology, Chosun University, Gwangju, Rep. of Korea. Also, he is a director of the IT Fusion Technology Research Center, Chosun University and an executive research director of the Public Welfare & Safety Research Program of the National Research Foundation of Korea. His research has focused on ubiquitous healthcare; human body communications and power transmission; and energy harvesting devices.

Seong-Ook Park received his BS degree from Kyungpook National University, Daegu, Rep. of Korea, in 1987; his MS degree from the Korea Advanced Institute of Science and Technology, Seoul, Rep. of Korea, in 1989; and his PhD degree from Arizona State University, Tempe, USA, in 1997, all in electrical engineering. From March 1989 to August 1993, he was a research engineer with Korea Telecom, Daejeon, Rep. of Korea, working on microwave systems and networks. He later joined the Telecommunication Research Center, Arizona State University, USA, until September 1997. Since October 1997, he has been with the Information and Communications University, Daejeon, Rep. of Korea, first as an associate professor, and currently as a professor at the Korea Advanced Institute of Science and Technology, Daejeon, Rep. of Korea. His research interests include mobile handset antenna and analytical and numerical techniques in the area of electromagnetics.